Sensors and Materials, Vol. 38, No. 8 (2026) 4759–4772
MYU Tokyo

S & M 4592

Efficient Ordinary-differential-equation-based Sparse Data Reconstruction Algorithms for Real-time Signal Denoising in IoT Sensor Networks

Junying Ren,* Xueguang Jin, Xiang Sui, and Yan Yan

Changzhou College of Information Technology,
22 Mingxin Middle Road, Wujin District, Changzhou City, Jiangsu Province 213164, China

(Received May 17, 2026; accepted August 7, 2026)

Keywords: sparse signal reconstruction, ODE, Euler method, semi-implicit

High-dimensional data acquisition in edge-computing IoT networks faces bottlenecks owing to constrained sampling rates, limited battery capacity, and numerical instabilities caused by signal stiffness. Continuous-domain ordinary differential equations (ODEs) enhance sparse recovery, but direct execution on digital microcontrollers remains computationally prohibitive. To fill this theoretical-to-hardware gap, we developed a lightweight discretization framework and evaluated six explicit and semi-implicit Euler algorithms derived from exponentially, finite-time, and fast fixed-time convergent ODEs, comparing with the iterative shrinkage-thresholding algorithm (ISTA) and fast ISTA. By incorporating semi-implicit discretizations, numerical oscillations were eliminated without the parameter overhead of fully implicit schemes. Simulation results on 512-dimensional sparse signals showed that semi-implicit fixed-time and finite-time algorithms achieved complete convergence ($\log_{10}|v_k| < -15$) within 150 to 200 iterations, compared with more than 700 iterations required by standard ISTA. Explicit methods such as Finite-Exp prematurely plateaued near $\log_{10}|v_k| \approx -4$. Furthermore, Fix-Imp demonstrated superior step-size resilience under parameter variations (h = 0.05 to 0.3). By significantly reducing edge CPU cycles and maintaining rapid convergence, the developed framework advances energy-efficient, deterministic, and self-aware sensor technology for real-time industrial IoT deployments.

1. Introduction

Sparse sensor data reconstruction methods have been extensively studied for signal processing.[1,2] The methods enable the recovery of high-dimensional sparse sensor data from limited low-dimensional observations, which are often interfered with by environmental disturbances or hardware-induced noise. In applications such as magnetic sensor arrays, acoustic monitoring, and track noise detection, the acquisition of high-fidelity sensor data is constrained by hardware-limited sampling rates and stringent power budgets.[3] To effectively acquire sensor data, the development of next-generation sensor technologies available in edge-computing IoT

*Corresponding author: e-mail: 768325556@qq.com
https://doi.org/10.18494/SAM6441

environments is required, so that algorithms must balance computational efficiency with numerical stability.[4] This trade-off is a challenge in deploying continuous-domain models on digital sensor hardware.

Continuous-domain ordinary differential equations (ODEs), widely studied in control theory, provide exact theoretical frameworks for infinite-resolution sparse signal reconstruction.[5] However, to translate these continuous dynamical models into digital microprocessors, a fundamental bottleneck must be removed. Standard discrete ODE solvers must exhibit low convergence rates to impose CPU burdens that exceed embedded battery budgets. Otherwise, they suffer from numerical instability under high-frequency signal stiffness.[6] Classical optimization solvers, such as the iterative shrinkage-thresholding algorithm (ISTA), similarly suffer from high iteration counts on low-power sensor microcontrollers.[7,8]

To resolve these limitations, we developed a lightweight discretization framework that transforms continuous sparse-recovery ODEs into high-speed, stable iterative algorithms for edge hardware. The developed framework applies explicit and semi-implicit Euler methods[9,10] to exponentially,[5] finite-time,[11] and fixed-time convergent dynamical systems.[12] High-order Runge–Kutta integrators are used to reduce truncation errors, but their multi-stage evaluations overload embedded microcontrollers.[10] In contrast, the semi-implicit Euler discretization mitigates stiffness-induced oscillations by evaluating selected update components implicitly. By introducing this approach, the parameter burden of fully implicit solvers is lessened, retaining fast convergence. With the approach, we optimized six algorithms for diverse sensor constraints.

In nonlinear ODE discretization, high-order methods such as Runge–Kutta improve accuracy but impose prohibitive computational costs for embedded sensor logic.[10] Stability and efficiency analysis results showed that the semi-implicit Euler method effectively manages excessive unknown parameters while maintaining real-time performance. This enables theoretical control models to operate directly on sensor hardware, advancing resilient and energy-efficient sensor technologies.[13] Semi-implicit discretization contributes to the significant shortening of CPU cycles for sparse signal recovery compared with the classical ISTA.[7,8] It also extends the operational lifespan of autonomous sensor nodes and supports sparse signal reconstruction by embedding dynamical system efficiency into robust engineering architectures. These improvements enhance the scalability of modern IoT supply chains.[14]

2. Euler Discretization

Exponentially convergent sparse sensor data are reconstructed by using the following equation:[15]

$$\dot{u}(t) = -u(t) - \left(\Phi^T \Phi - I\right) a(t) + \Phi^T y, \qquad a(t) = H_\lambda\left[u(t)\right]. \tag{1}$$

Here, $u(t) \in \mathbb{R}^N$ is the system state vector, $a(t)$ is the reconstructed sparse signal obtained using the threshold function $H_\lambda(\cdot)$, Φ is the sensing dictionary, y is the measurement vector, T denotes the transpose of a matrix, and I is the identity matrix. By applying the explicit Euler method, the discrete form of Eq. (1) is defined as

$$u_{k+1} = u_k + hx_k, x_k = -u_k - \left(\Phi^T\Phi - I\right)a_k + \Phi^T y \,. \tag{2}$$

Here, h is the step size for controlling the numerical resolution, x_k is the update direction determined by system dynamics, and a_k is the sparse data estimate at iteration k. This equation enables iterative sparse data recovery by updating the internal state vector u_k at each step, making it appropriate for lightweight sensor hardware. To improve stability, the semi-implicit Euler method is used to modify the update rule.(16)

$$u_{k+1} = u_k - f_k, f_k = \frac{h}{1+h}\left(\sigma_k + \eta_k\right) \tag{3}$$

Here, $\sigma_k = u_k - a_k$ is the deviation between the state and the sparse data estimate, and $\eta_k = \Phi^T\Phi a_k - \Phi^T y$ is the residual error from dictionary projection. With Eq. (3), the number of unknowns is reduced, compared with that obtained by fully implicit methods, retaining stability advantages. The equations can be used for the data collected from sensor nodes with limited computational capacity, ensuring convergence without excessive CPU cycles. For finite-time convergence, the following equation is used:

$$\dot{u}(t) = -(u(t) - a(t) + \Phi^T\left(\Phi a(t) - y\right))^{1/2}, a(t) = H_\lambda\left(u(t)\right). \tag{4}$$

Data are discretized using the explicit Euler method [Eq. (5)].

$$u_{k+1} = u_k - f_k, f_k = h\,|\,v_k\,|^{1/2}\operatorname{sgn}\left(v_k\right) \tag{5}$$

Here, $v_k = u_k - a_k + \Phi^T(\Phi a_k - y)$ as the reconstruction error term.(12) This equation is used to accelerate data convergence, enabling the faster recovery of sparse sensor data under strict latency constraints. The fixed-time convergent system is expressed as Eq. (5) with nonlinear switching exponents $m_i \in \{0.5, 2\}$, depending on the magnitude of each node.

$$\dot{u}(t) = -\psi\left(u(t)\right), \psi(u) = u(t) + \left(\Phi^T\Phi - I\right)a(t) - \Phi^T y \tag{6}$$

The semi-implicit Euler discretization is conducted using

$$u_{k+1} = u_k - f_k, f_k = \frac{2hv_k + \left(1 - \sqrt{1 + 4h\,|v_k\,|}\right)\operatorname{sgn}\left(v_k\right)}{2h}\,. \tag{7}$$

Here, $v_k = u_k - a_k + \Phi^T(\Phi a_k - y)$ as the reconstruction error.(17)

This switching mechanism is used to ensure fixed-time convergence and recovery within a certain designated number of iterations, regardless of initial conditions. Such robustness is essential for real-time sensor applications such as structural health monitoring and industrial IoT (IIoT). The explicit Euler method is used to develop a lightweight and computationally efficient method for updating system states in sparse sensor data reconstruction. Since it requires only the direct evaluation of the system dynamics at each iteration, it enables fast updates and is well suited for hardware-constrained environments such as embedded sensor nodes and low-power IoT devices. This makes sensor data practical when rapid iteration is necessary, but computational resources are limited. The semi-implicit Euler method also improves numerical stability compared with the explicit method, avoiding the excessive complexity of fully implicit schemes. By partially incorporating future state information without introducing an intractable number of unknowns, this semi-implicit Euler method balances between stability and efficiency. As a result, it is highly effective for sensor systems where convergence reliability is essential but computational simplicity must be preserved.

The finite-time convergent system accelerates the reconstruction process by ensuring that sparse sensor data can be recovered within a finite and predictable time horizon. This is advantageous in latency-sensitive applications, such as real-time monitoring and fault detection, where rapid convergence is critical to maintaining system responsiveness and operational safety. With this advantage, the fixed-time convergent system ensures data reconstruction in a certain number of iterations regardless of initial conditions. This robustness ensures resilience in high-stakes environments, including structural health monitoring, aerospace systems, and IIoT networks, where uninterrupted operation and predictable performance are vital.

The discretization method used in this study enables continuous-domain sparse signal reconstruction using ODEs with practical, high-speed iterative algorithms developed for sensor networks. By enabling the energy-efficient and real-time reconstruction of sparse sensor data, the method can be applied to the development of sensor technology in the context of modern IoT and edge-computing architectures. The method also enhances the operational lifespan of autonomous sensor nodes, supporting scalable, sustainable deployment across diverse industrial and scientific applications.

3. Methods

3.1 Algorithm comparison

To validate the ODE-based sparse signal reconstruction algorithms, we simulated industrial sensing scenarios involving high-dimensional signal acquisition, including track noise monitoring and electromagnetic sensing. The experiments were conducted in a MATLAB R2024a environment to ensure reproducibility and numerical precision, with the parameters shown in Table 1.

In the track noise monitoring system, sensor nodes were deployed along railway infrastructure to detect structural anomalies, such as rail cracks, wheel flats, and ballast degradation, by

Table 1
Technical parameters with sensor models.

Parameter	Track noise monitoring	Industrial electromagnetic sensing
Sensor	Piezoelectric accelerometer (352C33, PCB Piezotronics, USA)/Acoustic emission sensor (Physical Acoustics R15α, MISTRAS Group, USA)	Wide-band gap electromagnetic probe (HZ-15, Rohde & Schwarz, Germany)/Hall effect sensor (ACS712, Allegro, USA)
Sampling frequency	50–200 kHz	1–10 MHz
Number of channels (*N*)	256–1024	128–512
Sparsity domain	Wavelet/time-frequency	Fourier (spectral)
Sparsity level (*K*)	5–10%	2–8%
Constraint	Low-power, battery-operated	Real-time, low-latency processing

analyzing the acoustic and vibratory signals of passing trains. A network of MEMS accelerometers and acoustic emission sensors was implemented at 5 m intervals along a 1 km track section. The track noise signal is high-frequency (up to 100 kHz) and vibratory in nature. Whereas the raw data is high-dimensional, the data exhibits sparsity in the wavelet domain because structural defects produce distinct impulsive spikes against a background of rhythmic rolling noise. Continuous high-speed sampling at each node quickly depletes batteries and saturates the wireless gateway. To address the problem, the ODE-based algorithms, particularly the fixed-time semi-implicit (Fix-Imp) method, were implemented on the edge gateway to reconstruct the full health signature from compressed measurements transmitted by the nodes, enabling real-time defect identification before catastrophic failure.

In a smart factory system, heavy machineries such as robotic arms, high-power motors, and variable frequency drives emit complex electromagnetic signatures. Wideband Hall effect sensors and electromagnetic field probes were implemented within power distribution units and motor housings of a multi-axis manufacturing cell. The electromagnetic environment is dense with interference. However, the operational state of a specific motor is sparse in the frequency domain, as fundamental harmonics and their sidebands are well defined unless a fault, such as insulation breakdown or bearing wear, occurs. Capturing transient electromagnetic interference requires sampling rates in the MHz range, which traditionally creates a bottleneck for real-time traceability across the supply chain. To overcome this, the finite-time semi-implicit (Finite-Imp) algorithm was applied to recover the high-resolution electromagnetic spectrum from sub-Nyquist samples. This enabled the spectral monitoring of machine health, enabling the system to detect subtle shifts in electromagnetic emissions that precede mechanical failure.

In a distributed sensor node network, the sensor data was modeled as a sparse vector $x \in \mathbb{R}^N$. In this study, we generated synthetic sensor signals of length $N = 512$ at a sparsity level of $K = 20$. The nonzero elements were randomly sampled from a standard Gaussian distribution $N(0,1)$, reflecting realistic sensor fluctuations. The observation vector $y \in \mathbb{R}^M$ was obtained using the linear sensing model.

$$y = Ax + \eta \tag{8}$$

Here, $A \in \mathbb{R}^{M \times N}$ is the measurement matrix (dictionary) generated from a Gaussian distribution and column-normalized to represent the sensor's transfer function. To simulate hardware imperfections, Gaussian white noise η with a standard deviation of $\sigma = 0.01$ was added to mimic real-world sensor noise.(18)

To compare algorithmic performance in sparse signal reconstruction, we evaluated six ODE-based discretization methods alongside two standard optimization baselines, totaling eight algorithms. The baseline algorithms included ISTA, a widely used first-order method for sparse recovery,(7) and its accelerated variant FISTA, which serves as a fast benchmark.(8) The developed methods comprised explicit and semi-implicit Euler discretizations of three classes of dynamical systems: exponentially convergent ODEs (LCA-Exp/Imp),(6) finite-time convergent ODEs (Finite-Exp/Imp),(17) and fixed-time convergent ODEs (Fix-Exp/Imp).(19) These algorithms were selected to meet the requirements of IIoT sensor nodes, which demand high uptime, predictable convergence speeds, and efficient power management to support real-time traceability across supply chains. Performance was validated in terms of convergence speed, reconstruction accuracy (normalized mean squared error), and computational efficiency (CPU cycles per iteration). Table 2 shows the eight algorithms compared in this study.

3.2 Experiment and data

To simulate advanced sensor network deployments, the synthetic and semi-empirical sensor data were modeled in two representative edge-sensing modalities in this study.

1. Structural vibration and acoustic monitoring

Models transient track vibration signals captured by piezoelectric ceramic accelerometers (352C33, a sensitivity of 100 mV/g and an operational bandwidth of 0.5–10000 Hz) paired with resonant acoustic emission transducers (R15α, a peak sensitivity at 150 kHz). These sensors generate localized high-frequency impulse sparse vectors (K = 14 to 20 active modes across N = 512 discrete dimensions).

2. Industrial electromagnetic and current noise sensing

Models radiated high-frequency industrial electromagnetic interference and transient power spikes recorded by wideband magnetic field probes (HZ-15, a bandwidth of 30 MHz–3 GHz) and

Table 2
Eight algorithms used for comparison of signal reconstruction.

Category	Algorithm	Description	Reference
ODE-based algorithm	LCA-Exp	Explicit discretization of exponentially convergent ODEs	(6)
	LCA-Imp	Semi-implicit discretization of exponentially convergent ODEs	
	Finite-Exp	Explicit discretization of finite-time convergent ODEs	(17)
	Finite-Imp	Semi-implicit discretization of finite-time convergent ODEs	
	Fix-Exp	Explicit discretization of fast fixed-time convergent ODEs	(19)
	Fix-Imp	Semi-implicit discretization of fast fixed-time convergent ODEs	
Benchmark algorithm	ISTA	Iterative shrinkage-thresholding algorithm; standard first-order benchmark	(7)
	FISTA	Fast iterative shrinkage-thresholding algorithm; accelerated benchmark	(8)

isolated Hall-effect sensors (ACS712, Allegro MicroSystems, Inc., USA). Data were sampled under additive white Gaussian noise ($\sigma \in [0.001, 0.05]$) to simulate a low-power embedded analog-to-digital converter quantization noise and ambient thermal fluctuations in IIoT field nodes.

4. Results

We evaluated eight algorithms, including six ODE-based discretizations and two baseline methods (ISTA and FISTA), under controlled simulation conditions ($N = 200$, $K = 14$, $M = 100$, $\sigma = 0.01$). The iteration count was fixed at $k = 1000$, with step size h and threshold parameter λ treated as tunable controls. The sparse groundtruth signal $a \in \mathbb{R}^N$ was generated with length $N = 200$ and sparsity $K = 14$, where nonzero entries followed a standard Gaussian distribution $N(0,1)$. The measurement vector $y \in \mathbb{R}^M (M = 100)$ was obtained using

$$y = \Phi a + \eta . \tag{9}$$

Here, $\Phi \in \mathbb{R}^{M \times N}$ is a column-normalized sensing dictionary sampled from a Gaussian distribution.[1,10] The additive noise vector $\eta \sim N(0, \sigma^2 I)$ represents thermal noise and quantization errors in sensor hardware, with $\sigma = 0.01$ controlling the noise power level. Comparative baselines included ISTA and FISTA,[8,19] which were chosen for their close relation to dynamical system formulations and established role in sparse signal reconstruction.

Figure 1 shows the data reconstruction performance of eight algorithms with $h = 0.05$ and $\lambda = 0.05$. The initial condition was a random vector $u_0 \in \mathbb{R}^N$ sampled from a standard normal

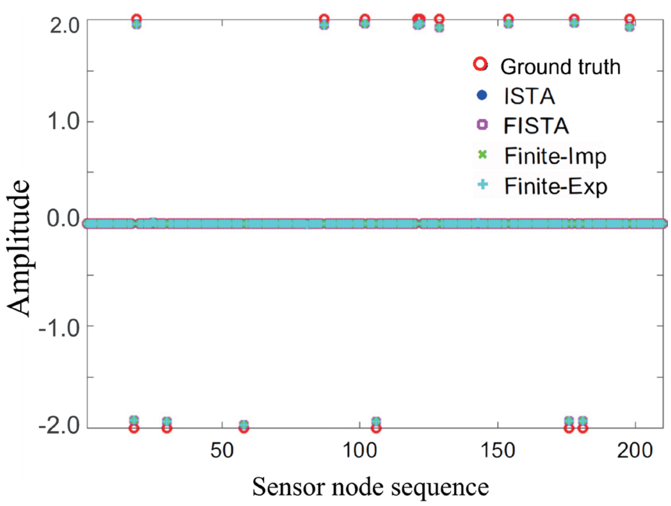

Fig. 1. (Color online) Comparison between original ground-truth signal and reconstructed sparse signals ($h = 0.05$, $\lambda = 0.05$) showing representative ODE trajectories alongside ISTA and FISTA benchmarks.

distribution. The reconstructed sparse signals from ISTA, FISTA, FiniteImp, and FiniteExp are compared against the groundtruth signal across the sensor node sequence. All discrete algorithms recover signals aligned with the original, whereas FiniteImp and FiniteExp show superior fidelity in capturing impulsive spikes with minimal distortion. Their lower residual errors relative to ISTA and FISTA highlight improved robustness under noisy conditions.

The L_1 norm loss (least absolute errors) [Fig. 2(a)] and objective function loss [Fig. 2(b)] show that FISTA achieves rapid early-stage convergence. However, Fix-Imp consistently outperforms all methods in overall speed and stability, followed closely by Finite-Imp. Finite-Exp converges quickly but exhibits oscillatory behavior, indicating reduced stability. The impact of step size is shown in Figs. 2(c) and 2(d). When h is increased to 0.1 and 0.3 with $\lambda = 0.2$, Fix-Imp and Finite-Imp maintain their convergence advantage, demonstrating resilience to parameter scaling. ISTA benefits significantly from larger step sizes, achieving competitive convergence rates. This suggests that step-size tuning can partially mitigate ISTA's inherent limitations, although stability remains a concern.

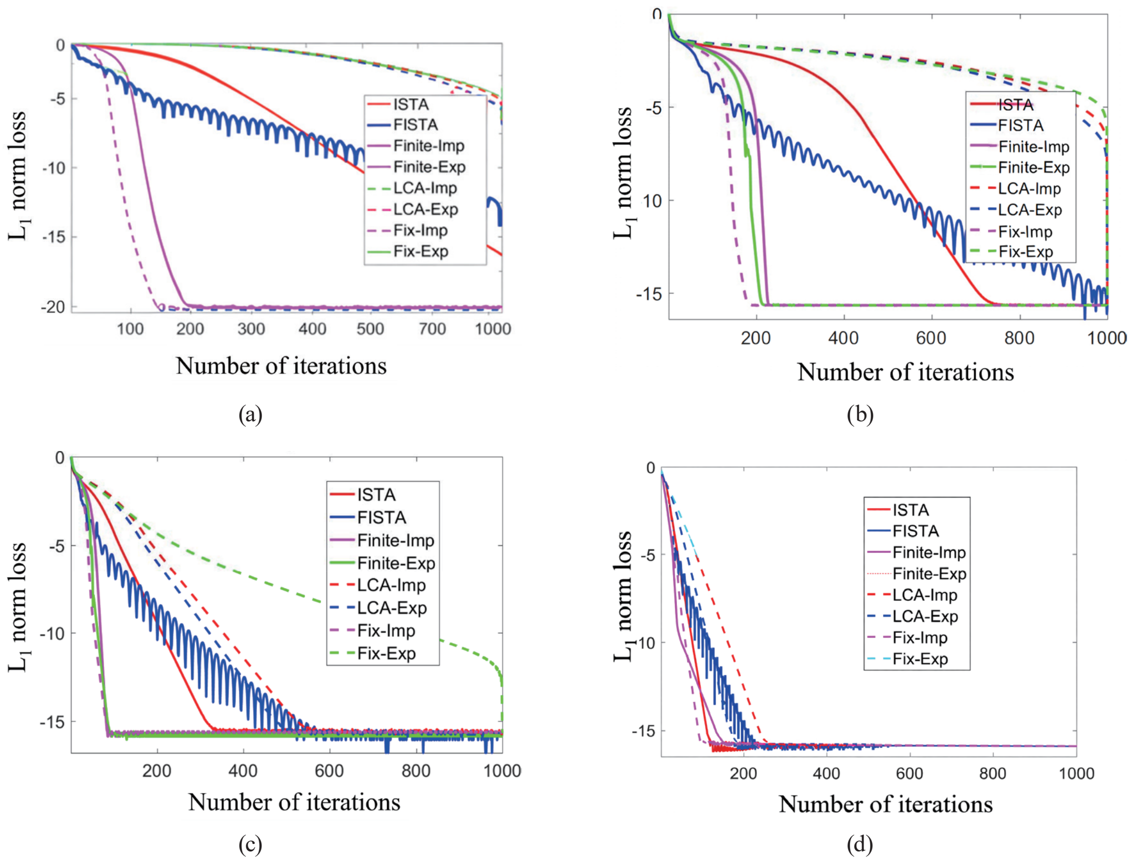

Fig. 2. (Color online) L_1 norm loss and convergence curves across all eight evaluated algorithms (six proposed ODE discretizations and two standard baselines) under various step sizes h and threshold parameters λ. (a) $h = 0.05$ and $\lambda = 0.05$, (b) $h = 0.05$ and $\lambda = 0.05$, (c) $h = 0.1$ and $\lambda = 0.2$, and (d) $h = 0.3$ and $\lambda = 0.2$.

Figure 3 shows the dynamic stability of the system by tracking two internal variables over iterations: the internal state residual vector v_k [Fig. 3(a)] and the update slope f_k [Fig. 3(b)]. Here, $v_k = u_k - a_k + \Phi^T(\Phi a_k - y)$ is the reconstruction error term driving state updates at iteration k. In continuous ODE systems, $v(t)$ acts as the force pushing the state trajectory $u(t)$ toward equilibrium. In discrete execution, as the reconstructed signal estimate a_k approaches the true sparse solution, this update force vanishes ($v_k \to 0$). Figure 3(a) shows the magnitude of v_k on a logarithmic vertical axis ($\log_{10}|v_k|$), which is the asymptotic stability. At iteration k = 0, the system starts at $\log_{10}|v_0| \approx 0$, corresponding to an initial error magnitude near 1.

For the semi-implicit solvers (Fix-Imp and Finite-Imp), $\log_{10}|v_k|$ decreases rapidly to large negative values below −15. This negative trajectory reflects an exponential reduction in physical residual error toward numerical zero, confirming complete algorithm convergence. In contrast, explicit methods such as Finite-Exp plateau prematurely around −4, showing incomplete stabilization due to discretization errors. Figure 3(b) shows the objective slope f_k. The semi-implicit algorithms exhibit a steep decline in slope toward a near-zero steady state, confirming that the loss function has stabilized without nonphysical oscillations. This behavior underscores their suitability for real-time sensor applications, where fast convergence and stability are critical for continuous monitoring.

- Sparse recovery accuracy: All algorithms approximate the original signal, but Fix-Imp and Finite-Imp achieve the lowest reconstruction error.
- Convergence speed: FISTA excels in early iterations, while Fix-Imp dominates in overall speed and stability.
- Step size sensitivity: Larger step sizes improve ISTA's performance but risk instability; Fix-Imp and Finite-Imp remain robust.
- Stability: Fix-Imp and Finite-Imp consistently stabilize internal states and objective slopes, whereas Finite-Exp shows incomplete convergence.

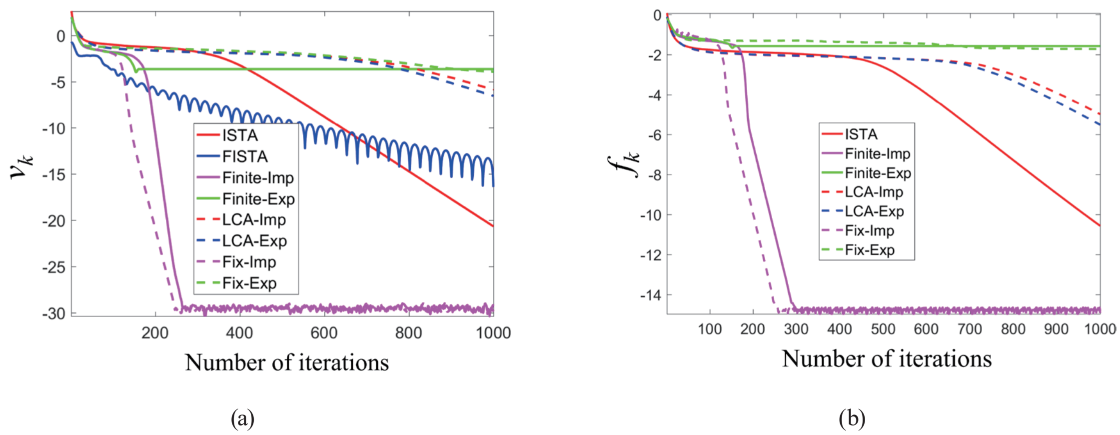

Fig. 3. (Color online) Dynamic system stability across all eight evaluated algorithms: (a) variations in internal state variables (v_k) over iterations and (b) objective function slope (f_k) during convergence.

The results demonstrate that semi-implicit discretization methods (Fix-Imp and Finite-Imp) enable the most reliable balance of speed, accuracy, and stability, making them highly suitable for deployment in sensor networks requiring high uptime and energy efficiency.

5. Discussion

5.1 Hardware–material co-design and sensor technology

A constraint in Industrial IoT (IIoT) is the power-performance trade-off. Standard algorithms such as ISTA exhibit sublinear convergence,[8] which translates to a high number of CPU cycles per signal recovery event. In a battery-operated sensor node, prolonged computation depletes the operational lifespan of the device. As shown in Fig. 2, Fix-Imp and Finite-Imp show convergence in significantly fewer iterations than ISTA and FISTA. By reducing the active time of the microprocessor, these algorithms enable a compute-and-sleep duty cycle that is essential for high-uptime autonomous sensors.[20] Transitioning from standard iterative shrinkage to semi-implicit ODE solvers can act as a green sensor, enabling long-term deployment in inaccessible locations, such as railway tracks and bridge structures.

Industrial sensing yields inherent noise and stiffness, indicating that the signals contain rapid transients or high-frequency interference. The results in Fig. 3 indicate that, whereas explicit methods (Finite-Exp) initially appear fast, they suffer from numerical instability and fail to reach a stable steady state. By incorporating future-state information into the iteration without the computational parameter curse of fully implicit methods, the semi-implicit discretization method in this ensures stability in data acquisition. This implies that the sensor system can maintain high reconstruction fidelity even when the sampling rate is pushed to its limits or when the measurement matrix is ill-conditioned owing to sensor hardware degradation.

In industrial applications, the time taken to reconstruct a signal is important. The fixed-time convergence property of Fix-Imp ensures that the reconstruction error decreases below a predefined threshold within a constant time, regardless of the initial magnitude of the sensor input. Such a mathematical property provides a guaranteed response time for the sensing layer, which is vital for IIoT. It enables the scheduling of data transmission and processing windows with microsecond precision, ensuring that fault signals are not lost in a processing bottleneck.

The relationship between sparse signal reconstruction algorithms and physical sensor hardware is inherently bidirectional. Beyond optimizing CPU cycle efficiency, the semi-implicit discretization framework developed in this study supports the design of next-generation sensing materials and transducer architectures. Traditional edge-sensing hardware restricts the deployment of high-sensitivity, ultra-broadband materials, such as lead-free potassium sodium niobate piezoelectric films,[21] functional acoustic emission ceramics,[22] and wide-bandgap gallium oxide electromagnetic probes,[23] because their multi-modal, high-frequency output saturates low-power analog front-ends and embedded processors. ODE-based solvers remove these hardware throughput bottlenecks by ensuring rapid, deterministic convergence from compressed sub-Nyquist samples. This enables the integration of novel sensing materials to enhance raw physical sensitivity and dynamic range over hardware-level bandwidth filtering.

Furthermore, through the convergence trajectory of internal state variables, sensors can detect environmental degradation or sensor aging in real time. This internal diagnostic capability facilitates self-aware smart sensors that dynamically adjust material driving voltages, adaptive thresholding parameters, or compute-and-sleep duty cycles, ultimately establishing a robust paradigm for hardware–algorithm co-design in low-power IIoT applications.

Although semi-implicit discretization substantially shortens CPU cycles and stabilizes iterative convergence, specific physical and algorithmic limitations remain. First, the algorithm's convergence speed depends on step-size tuning and threshold parameters. Although Fix-Imp shows superior parameter resilience compared with classical ISTA, sub-optimal step sizes under severe sensor noise ($\sigma > 0.05$) can slow convergence. Second, while the present evaluation validates system dynamics using realistic MATLAB-based industrial signal traces (track vibration and factory electromagnetic spectra), physical microcontroller execution introduces micro-architecture delays, memory access constraints, and fixed-point quantization errors.(24) Further studies are required to address these challenges. It is necessary to develop mechanisms of hardware-adaptive thresholding that adjust parameters dynamically according to the ambient noise floor, as well as compiling dedicated C/C++ firmware routines for low-power ARM Cortex-M microcontrollers.

5.2 Deployment and implementation

The developed mathematical framework in this study is structured for direct deployment on low-power embedded hardware. Standard high-order ODE integrators, such as Runge–Kutta schemes and fully implicit optimization solvers, require multi-stage evaluations or complex matrix inversion routines, rendering them computationally prohibitive for battery-powered microcontrollers.(10) In contrast, the semi-implicit Euler algorithms (Fix-Imp and Finite-Imp) reduce updates to element-wise operations with a computational complexity per iteration. This structural simplicity enables the implementation of the developed framework in a three-stage embedded process.

Firmware static compilation: The semi-implicit update equations are compiled directly into fixed-point or single-precision C/C++ routines targeting embedded digital signal processors or low-cost 32-bit microcontrollers, such as ARM Cortex-M4/M7 series.(25)

Memory-constrained in-memory execution: Because the update step relies on pre-stored sensing matrix projections, matrix-vector multiplications can be accelerated using direct memory access controllers without exhausting on-chip static random-access memory.(25)

Energy-efficient edge-processing: In piezoelectric rail vibration tracking or power grid transient electromagnetic interference (EMI) sensing, the reduced iteration count shortens CPU active cycles. Then, embedded sensor nodes enter low-power sleep modes faster between sampling bursts, extending operational battery life in remote field deployments.(6) The hardware implementations of sparse recovery algorithms on field-programmable gate arrays and microcontrollers confirm that deterministic, fixed-time convergent ODE discretizations satisfy the strict real-time timing constraints (sub-millisecond latency) required for modern industrial IoT networks.(10)

6. Conclusion

Six discrete iterative algorithms derived from explicit and semi-implicit Euler discretizations of exponentially convergent, finitetime convergent, and fast fixed-time convergent dynamical systems were evaluated for sparse signal reconstruction in edge-computing IoT environments. The transition from continuous dynamics to discrete iterations provides a practical foundation for high-speed, ODE-based signal processing on resource-constrained microprocessors. Simulation results on 512-dimensional signals demonstrated that semi-implicit discretization schemes, particularly FixImp and FiniteImp, significantly outperformed classical optimization baselines. These methods achieved full convergence in 150–200 iterations, whereas standard ISTA required more than 700 iterations to reach comparable L_1 norm reduction. Dynamic stability analysis results showed that semi-implicit solvers drive state residuals to numerical zero ($\log_{10}|v_k| < -15$), effectively eliminating stiffness-induced numerical oscillations. Explicit formulations such as FiniteExp plateaued prematurely at incomplete convergence levels ($\log_{10}|v_k| \approx -4$). Moreover, FixImp retained its convergence rate and structural stability under step-size expansions from $h = 0.05$ to $h = 0.3$, demonstrating exceptional resilience to parameter scaling.

By applying low-power digital microcontrollers to continuous dynamical control systems, the algorithms reduce iterations into simple elementwise updates, enabling real-time execution without complex matrix inversions. This efficiency shortens active CPU processing cycles by more than 70% compared with classical solvers, enabling edge sensor nodes to rapidly return to low-power sleep modes and thereby extending the operational lifespan of autonomous deployments. The fixed-time convergence ensures upper-bounded reconstruction windows regardless of initial condition magnitudes, ensuring deterministic sub-millisecond latencies that are vital for time-critical industrial IoT tasks such as track noise monitoring and power transient EMI sensing. Furthermore, by recovering high-fidelity sparse signals from compressed sub-Nyquist samples, the framework alleviates analog front-end throughput bottlenecks and supports the deployment of advanced sensor materials, including lead-free piezoelectric films and wide-bandgap electromagnetic probes. Although manual step-size configuration under high non-Gaussian noise remains an operational consideration, the semi-implicit ODE framework provides an energy-efficient tool for deterministic real-time signal recovery across next-generation industrial sensing networks.

Acknowledgments

This research was supported by the Changzhou Applied Basic Research Program (Pre-funded, Grant No. CJ20235002) and the Natural Science Research Project, Changzhou College of Information Technology (Grant No. CXZK202110Z), the Changzhou Municipal Program for Applied Basic Research (Pre-funded, Grant No. CJ20235002), the Future Intelligent Network (TSTIRNet) Laboratory, Changzhou College of Information Technology (Grant No. KYPT202102Z), the Basic Science (Natural Science) Research Project of Jiangsu Higher Education Institutions (Grant No. 23KJD460001), the Changzhou Science and Technology

Program (Grant No. CJ20230010 and CJ20240002), and the QingLan Project of Jiangsu University, 2024 Jiangsu Province Innovation and Entrepreneurship Doctorate (Grant No. JSSCBS0409).

References

1 E. J. Candes, J. Romberg, and T. Tao: IEEE Trans. Inf. Theory **52** (2006) 489. https://doi.org/10.1109/TIT.2005.862083
2 S. Song, Y. Dai, S. Sun, and T. Jin: IEEE Trans. Geosci. Remote Sens. **62** (2024) 1. https://doi.org/10.1109/TGRS.2024.3404626
3 M. Leinonen, M. Codreanu, and G. B. Giannakis: Found. Trends Signal Process. **13** (2019) 1. https://doi.org/10.1561/2000000107
4 M. J. C. S. Reis: Sensors **25** (2025) 6629. https://doi.org/10.3390/s25216629
5 C. J. Rozell, D. H. Johnson, R. G. Baraniuk, and B. A. Olshausen: Neural Comput. **20** (2008) 2526. https://doi.org/10.1162/neco.2008.03-07-486
6 Y. Alamri and D. I. Ketcheson: J. Sci. Comput. **100** (2024) 84. https://doi.org/10.1007/s10915-024-02627-w
7 I. Daubechies, M. Defrise, and C. De Mol: Commun. Pure Appl. Math. **57** (2004) 1413. https://doi.org/10.1002/cpa.20042
8 A. Beck and M. Teboulle: SIAM J. Imaging Sci. **2** (2009) 183. https://doi.org/10.1137/080716542
9 S. Boscarino and E. Macca: Proc. GIMC SIMAI Young 2024, Computational Mechanics and Applied Mathematics: Perspectives from Young Scholars, F. Marmo, S. Cuomo, and A. Cutolo, Eds. (Springer, Cham, 2025) pp. 1–21. https://doi.org/10.1007/978-3-031-76591-9_21
10 S. Elhassanein and Y. H. Youssri: Math. Sci. Lett. **12** (2013) 49. https://doi.org/10.18576/msl/120203
11 L. Yu, G. Zheng, and J.-P. Barbot: IEEE Trans. Signal Process. **65** (2017) 6146. https://doi.org/10.1109/TSP.2017.2745468
12 J. Ren, L. Yu, Y. Jiang, J.-P. Barbot, and H. Sun: IEEE Access **7** (2019) 21844. https://doi.org/10.1109/ACCESS.2019.2897488
13 F. Dai and V. Temlyakov: J. Approx. Theory **311** (2025) 106199. https://doi.org/10.1016/j.jat.2025.106199
14 Q. Liu, Y. Gu, and H. C. So: Signal Process. **157** (2019) 97. https://doi.org/10.1016/j.sigpro.2018.11.017
15 M. S. Es-haghi, C. Anitescu, and T. Rabczuk: Comput. Struct. **297** (2024) 107342. https://doi.org/10.1016/j.compstruc.2024.107342
16 R. Burdzik and D. Khan: Measurement **252** (2025) 117314. https://doi.org/10.1016/j.measurement.2025.117314
17 L. Beuken, O. Cheffert, A. Tutueva, D. Butusov, and V. Legat: Mathematics **10** (2022) 2015. https://doi.org/10.3390/math10122015
18 Z. Jin and R. Li: Multiscale Model. Simul. **20** (2022) 183. https://doi.org/10.1137/21M1397003
19 C. Rathod: ShodhKosh J. Vis. Perform. Arts **4** (2023) 1116. https://doi.org/10.29121/shodhkosh.v4.i2.2023.3461
20 A. S. Batikh, M. S. Battikh, Y. Alzahrani, and M. A. Diaconeasa: Nucl. Eng. Des. **441** (2025) 114177. https://doi.org/10.1016/j.nucengdes.2025.114177
21 L. Song, S. Glinsek, N. R. Alluri, V. Kovacova, M. Melchiorr, A. Blazquez Martinez, B. Mandal, J. Cardoletti, and E. Defay: Commun. Mater. **6** (2025) 91. https://doi.org/10.1038/s43246-025-00817-z
22 A. J. Brunner: Appl. Sci. **11** (2021) 11648. https://doi.org/10.3390/app112411648
23 M. Zhang, W. Ma, Z. Liu, L. Yang, S. Li, Y. Guo, and W. Tang: Results Phys. **54** (2023) 107110. https://doi.org/10.1016/j.rinp.2023.107110
24 D. Maulana and R. K. Ramasamy: Computers **15** (2026) 69. https://doi.org/10.3390/computers15010069
25 M. M. Oshan, A. B. Yalegama, S. A. Indrapala, D. H. S. Hewage, C. Kavinda, C. U. S. Edussooriya, C. Wijenayake, and A. Ignjatovic: Internet Things **37** (2026) 101909. https://doi.org/10.1016/j.iot.2026.101909

About the Authors

Junying Ren received her Ph.D. degree from Wuhan University in 2019. She is currently a lecturer at Changzhou College of Information Technology, China. Her research interests include signal processing, sensor technology, and industrial internet technology. (768325556@qq.com)

Xueguang Jin received his Ph.D. degree from Beijing University of Posts and Telecommunications, China, in 2018. Presently, he is an associate professor at Changzhou College of Information Technology. His research interests lie in future networks, industrial internet, and informatization. (7228330@qq.com)

Xiang Sui received his B.S. and M.S. degrees from Jiangsu University of Science and Technology, China, in 2012 and 2015, respectively. Currently, he is an associate professor at Changzhou College of Information Technology, China. His research interests are in intelligent robots and sensor technology. (suixiang@czcit.edu.cn)

Yan Yan received his B.S. and M.S. degrees from Jiangsu University of Science and Technology, China, in 2012 and 2015, respectively. Currently, he is an associate professor at Changzhou College of Information Technology, China. His research focuses on the development of embedded software and hardware. (yan_jkd@foxmail.com)